UV integrated photonics in sputter deposited aluminum oxide

WARD A. P. M. HENDRIKS, DAWSON B. BONNEVILLE, SOHEILA MARDANI, MEINDERT DIJKSTRA AND SONIA M. GARCIA-BLANCO*

Integrated Optical Systems (IOS) Group, MESA+ Institute for Nanotechnology, University of Twente, Enschede, 7500AE, The Netherlands
**Corresponding author: s.m.garciablanco@utwente.nl*

Received XX Month XXXX; revised XX Month, XXXX; accepted XX Month XXXX; posted XX Month XXXX (Doc. ID XXXXX); published XX Month XXXX

Abstract

Ultraviolet operating photonic integrated circuits (UV-PICs) can have large impact in application fields including UV Raman spectroscopy, UV-VIS spectroscopy, microscopy, metrology and quantum technology. In this work, we introduce a polycrystalline Al_2O_3 integrated photonic platform exhibiting ultra broadband operation from the ultraviolet (~200 nm) till the mid-IR (~3 μm) with very low propagation losses (i.e., 1.3 dB/cm at 369 nm of wavelength for TM polarization). Propagation loss characterization of channel waveguides with different widths revealed sidewall roughness as major contributor to the losses, paving the way for further future optimization of the devices.

1. Introduction

Applications operating in the ultraviolet wavelength range (i.e., between 200 and 400 nm), including UV Raman spectroscopy [1], UV-VIS spectroscopy [2], microscopy [3], metrology [4] and quantum computers based on trapped-ions/cold atoms [5], could potentially benefit from the scalability, increased robustness and efficiency, and reduced size and cost provided by photonic integration [6]. Most mature low-loss integrated photonic platforms, such as silicon nitride, cannot operate in such wavelength range due to their small bandgap, which leads to prohibitively high waveguide absorption losses below 450 nm [7]. Benefiting from waveguide structures with low confinement, recent demonstrations have shown losses below 1 dB/cm at 405 nm of wavelength in a silicon nitride waveguide of cross-section 24 nm by 800 nm, with negligible bending losses for radii around 1.3 mm [8]. Similar structures have been utilized to demonstrate injection locked lasers at a wavelength of 410 nm by combining an AlGaInN Fabry Perot laser hybrid coupled to a Si_3N_4 photonics integrated circuit (PIC) [9]. Another demonstration of such injection locking scheme has led to a tunable laser operating at a central wavelength of 404 nm, with a tuning range of 1.6 nm and an off-chip output power of 10 mW at 405 nm [10].

Alternative material platforms suitable for photonic integrated circuits operating below 400 nm are the III-nitrides (i.e., AlN and AlGaN) [11], silicon oxynitride (SiOxNy) [12, 13], and aluminium oxide (Al_2O_3) [14, 15, 16] thanks to their large bandgap of <200 nm [11, 17]. The high propagation losses demonstrated so far in the AlN platform, ranging from 60.4 dB/cm at 369.5 nm wavelength [18] to 8 dB/cm at 390 nm of wavelength for a similar waveguide cross-section [19], prevents it yet from serving useful applications in the UV wavelength range. On the other hand, the low-refractive index contrast of the SiOxNy prevents it from reaching the desirable high levels of photonic integration.

Al_2O_3 is an excellent material for integrated photonics thanks to its large transparency window from the ultraviolet till the mid-IR, low propagation losses and high solubility for rare-earth ions, allowing for optical gain at different wavelength ranges (i.e., ~1 μm [20], 1.3 μm [21], ~1.532 μm [22], and ~2 μm [23]). Amorphous AlOx films deposited by atomic layer deposition (ALD) have shown propagation losses as low as 4 dB/cm at a wavelength of 250 nm [24]. Amorphous AlOx single mode channel waveguides exhibited propagation losses of ~3 dB/cm at a wavelength of ~370 nm [14]. High confinement waveguides (i.e., confinement of ~0.9) have shown losses as low as 0.8 dB/cm [25] A record low propagation loss of 0.84 dB/cm at 390 nm has been reported, although in a very low confinement waveguide, which, again, limits the achievable integration density [15]. Amorphous Al_2O_3 cannot withstand temperatures above 800 °C as formation of polycrystalline γ-phase leads to losses in excess of 20 dB/cm [14]. A limited thermal budget prevents further processing steps known to reduce propagation losses, including the deposition of a high quality low-pressure vapor deposition (LPCVD) SiO_2 cladding and various annealing steps [26,27].

In this work, we present low-loss Al_2O_3 waveguides deposited by RF reactive sputtering. By controlling the deposition conditions, a nanocrystalline structure capable of withstanding temperatures in excess of 1100 °C without degradation of the optical performance is obtained. Channel waveguides with propagation losses as low as ~1.3 dB/cm at a wavelength of 369 nm for TM polarization and 2.3 dB/cm at 369 nm for TE polarization are experimentally demonstrated in medium confinement (37 %) waveguides of cross-section 70 nm x 750 nm, which can bend to radii <100 μm.

2. Fabrication

Al_2O_3 layers with a thickness of ~95 nm are deposited using an AJA ATC 15000 RF reactive co-sputtering system on 100 mm diameter silicon wafers with 8 µm thick thermal oxide. An aluminium target (Al, 99.9995 % purity) is utilized, to which a constant power of 200 W is applied [28]. The parameters used for the deposition of the Al_2O_3 layers utilized in this work are shown in Table 1. Prior to each deposition, the oxygen flow and substrate set temperature are optimized to yield as low as possible slab losses.

Table 1 Optimized RF reactive sputtering process parameters

Parameter	Value	Unit
Argon flow	30	sccm
Oxygen flow	3.1-3.2	sccm
Pressure	3.8	mTorr
Substrate set temperature	720-760	ºC
RF power to Al target	200	W

3. Slab waveguide characterization

The slab propagation losses were measured using a prism coupler setup (Metricon 2010M) with fiber loss tool. A propagation light streak at 377 nm on an as-deposited layer is shown in Figure 1 (a). Figure 1 (b) shows the exponential fit to the decay of the scattered light along the streak, which reveals slab propagation losses of ~0.40 ± 0.05 dB/cm at 377 nm.

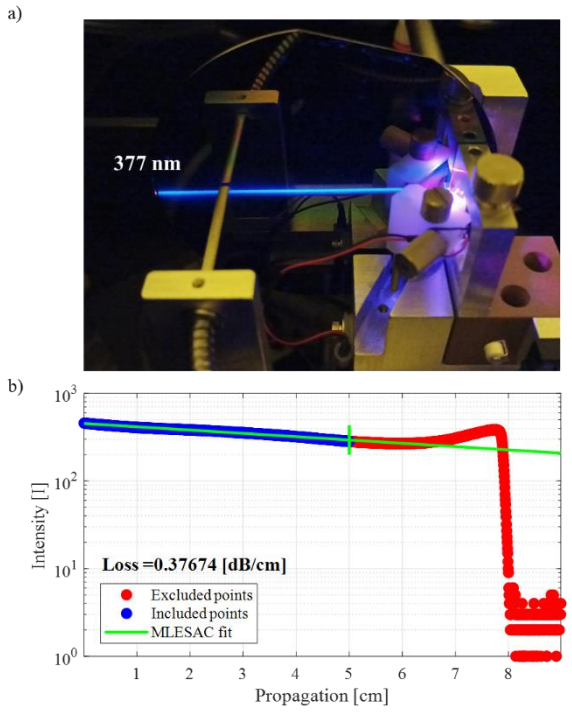

Figure 1 (a) Streak of light propagating through a ~70 nm thick slab waveguide (wavelength 377 nm); (b) Fit of the exponential decay of the propagating streak, showing a slab propagation loss of ~0.40 ± 0.05 dB/cm.

The thickness and refractive index were measured using variable angle spectroscopic ellipsometry (VASE) with a Woollam M-2000UI ellipsometer on a similar Al_2O_3 layer deposited on a bare silicon substrate. Figure 2 shows the spatial variation across the wafer revealing a thickness uniformity of 1–4 % and refractive index uniformity of <1 % in (a) and (b) respectively. The surface roughness of the as deposited layer was measured to be ~1.5 nm RMS using a Bruker Fast Scan AFM in scan-assist mode, over a scanned area of 500 x 500 nm². The layer was subsequently polished using chemical mechanical polishing (CMP) to a surface roughness of <0.2 nm RMS and final thickness of 70 nm.

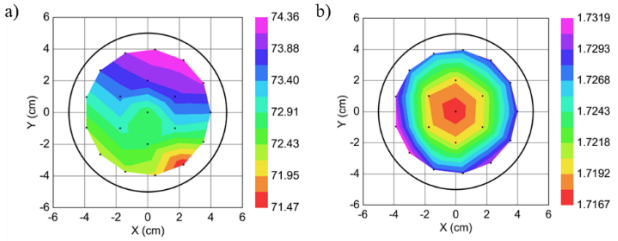

Figure 2. a) Thickness and b) refractive index mapped spatially across x and y coordinates on the wafer.

VASE down to VUV wavelengths was utilized to measure the optical constants necessary to calculate the bandgap of the Al_2O_3 deposited layers. To remove the influence of the SiO_2 undercladding from the measurements, the experiment was done on layers directly deposited on bare Si wafers. A bandgap of approximately 7.2 ev, corresponding to ~170 nm, was obtained.

3. Channel waveguide fabrication

Electron-beam lithography (EBL) was used to pattern negative resist (AR-N7520.18) at a dose of 2000 µC/cm² and acceleration voltage of 100 keV to be used as an etch mask for the definition of spirals of different lengths for propagation loss measurements using the cut-back method. Reactive ion-etching (RIE) was performed to define the waveguides. Low pressure chemical vapor deposition (LPCVD) was used to deposit a 1 µm of SiO_2 cladding at a deposition rate of 37 nm/min using 200 and 710 sccm of SiH_4/N_2 and N_2O respectively, with a chamber pressure of 650 mTorr at a temperature of 800 °C. Finally, an annealing step at 1150 °C for 3 h in nitrogen atmosphere followed by deposition of 7 µm of SiO_2 by plasma enhanced chemical vapor deposition (PECVD) was carried out before singulating the PICs with a diamond blade (f1230).

3. Channel waveguide characterization

Waveguide measurements were performed with piezo controlled stages and multiple laser sources at different wavelengths in the UV and short visible wavelengths. Polarization maintaining single mode fibers (i.e. 405 nm) were used to launch quasi-transverse electric (TE) and quasi-transverse magnetic (TM) modes at 369, 405 and 452 nm wavelengths into the nano-tapered edge couplers with a mode size diameter of 3.3 ± 0.5 µm². The cut-back method was used to extract the waveguide losses from transmission measurement of spirals ranging from ~3–15 cm in length, for three different widths of 550, 750, and 850 nm and a thickness of 70 nm. The waveguide propagation losses are summarized in Figure 3 (a) with images of the waveguides under measurement in Figure 3 (b), highlighting a record loss of 1.3 dB/cm at 369 nm of wavelength for TM operation for waveguides of width 750 nm.

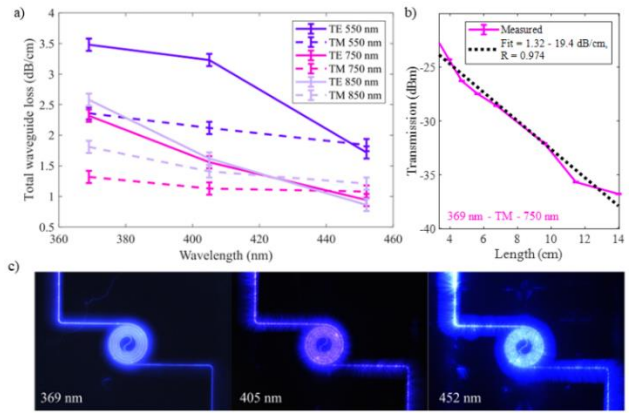

Figure 3. a) Total waveguide propagation loss measured via the cut-back method for varying waveguide widths, at 369, 405 and 452 nm for TE and TM polarization. The thickness of the waveguides was 70 nm in all three cases. (b) Image of light of different wavelengths (i.e., 369, 405 and 452 nm) propagating in a waveguide with cross-section 750 nmx70 nm.

A high coupling loss was observed for the waveguides, ranging from 5 dB (i.e., best case) to 30 dB per facet (i.e. worst case). Such high propagation losses result mainly from a bias between the design dimension of the nano-tapers with respect to the fabricated dimensions. The variability is most likely due to roughness and edge damage from a non-optimized dicing and polishing process. Intense efforts are currently underway to mitigate these issues with the development of proximity error correction (PEC) for the electron-beam lithography process and alternative facet formation techniques, which will be reported in a later publication.

The lower losses measured for TM modes compared to TE modes is due to the lower overlap of the TM modes with the sidewalls of the etched waveguide, which are the main contributors to scattering induced losses [7]. This also explains the higher losses for the 550 nm wide waveguides, which have higher overlap of the propagating mode with the sidewalls compared to the wider cross sections. The larger losses observed for the wider cross-section are associated to the appearance of higher order modes. From these measurements, we conclude that the major contributing factor to loss in the reported Al_2O_3 waveguides is sidewall roughness induced scattering, and not material bulk scattering or absorption. Future work will consider shorter and longer wavelengths with a larger variety of cross sections to better understand the different contributing factors to loss [7], and pathways towards minimizing it by optimizing the fabrication procedure.

4. Conclusion

We have demonstrated low loss Al_2O_3 waveguides in the UV and short visible wavelength range fabricated by RF reactive sputtering. The deposited films show slab propagation losses as low as 0.4 dB/cm at 377 nm. Layer uniformity below 4 % and a bandgap of 7.2 eV (170 nm) were characterized by VASE. Finally, propagation losses for a variety of widths and wavelengths were characterized by the cut-back method. A record low loss of 1.3 dB/cm has been achieved for TM modes at 369 nm. This, along with low losses at 405 and 452 nm, establishes Al_2O_3 as an enabling technology for a variety of applications where operation down to the ultraviolet and short visible wavelengths is required, such as UV Raman spectroscopy, UV-VIS spectroscopy, metrology and quantum computers based on trapped-ions/atoms.

Funding. This project has received support from the European Research Council Proof-of-concept grant (project number 964006), and from EIC Transition project ALUVia, which has received funding from the European Union's Horizon Europe research and innovation programme under grant agreement No. 101099699.

Acknowledgments. The authors thank Ivo Hegeman for assistance in the mask design utilized for the cut-back method.

Disclosures. The authors declare no conflicts of interest. Views and opinions expressed are however those of the author(s) only and do not necessarily reflect those of the European Union or the European Innovation Council. Neither the European Union nor the granting authority can be held responsible for them.

Data availability. Data underlying the results presented in this paper are not publicly available at this time but may be obtained from the authors upon reasonable request.

References

1. P.C., "Ultraviolet (UV) Raman Spectroscopy," in: Wachs, I.E., Bañares, M.A. (eds) Springer Handbook of Advanced Catalyst Characterization. Springer Handbooks. Springer, Cham (2023).
2. H. Perkampus, "UV-VIS spectroscopy and its applications, " in Springer Berlin Heidelberg, Germany (2013).
3. C. Lin, J.S.D. Peñaranda, J. Dendooven, *et al.,* Nat Commun **13**, 4360 (2022).
4. S. D. Bennett, E. A. Peltzer and I. R. Smith , Proc. SPIE **0897** (1988).
5. K. K. Mehta, C. Zhang, M. Malinowski, *et. al.,* Nature **586**, 533 (2020).
6. D. J. Blumenthal, APL Photonics **5**, 2 (2020).
7. M. Corato-Zanarella, X. Ji, A. Mohanty, *et. al*., Opt. Express **32**, 5718 (2024).
8. J. T. Morin, L. Chang, W. Jin, *et. al.,* Optica **8**, 755 (2021).
9. A. Siddharth, T. Wunderer, G. Lihachev, A, *et. al*., APL Photonics **7**, 046108 (2022).
10. M. Corato-Zanarella, A. Gil-Molina, X. Ji, *et. al*., Nat. Photon. **17**, 157 (2023).
11. M. Soltani, R. Soref, T. Palacios, *et. al.,* Opt. Express **24**, 25415 (2016).
12. K. B. Mogensen, P. Friis, J. Hübner, *et. al.,* Opt. Lett. **26**, 716 (2001).
13. R. Kervazo, L. Bodiou, J.-C. Simon, *et. al.,* Proc. SPIE **12148** (2022).
14. G. N. West, W. Loh, D. Kharas, *et. al*., APL Photonics **4**, 026101 (2019).
15. C. He, Y. Wang, C. Waldfried, *et. al*.," Opt. Express **31**, 33923 (2023).
16. W. A. P. M. Hendriks, L. Chang, C. I. Van Emmerik, *et. al*., Adv. Phys. X **6**, 1833753 (2021).
17. E. O. Filatova and A. S. Konashuk, J. Phys. Chem. C **119**, 20755 (2015).
18. W. Shin, Y. Sun, M.Soltani, *et. al.,* Appl. Phys. Lett. **118**, 211103 (2021).
19. X. Liu, A. W. Bruch, Z. Gong, *et. al.,* Optica **5**, 1279 (2018).
20. M. De Goede, L. Chang, J. Mu, *et al*., Opt Lett. **44**, 5937 (2019).
21. J. Yang, K. van Dalfsen, K. Worhoff, *et al*., Appl Phys B. **101**, 119 (2010).
22. J. Mu, M. Dijkstra, J. Korterik, et. al., Photon. Res. **8**, 1634 (2020).
23. N. Singh, J. Lorenzen, M. Sinobad. *Et al.* Nat. Photon. In press. (2024).
24. M. M. Aslan, N. A. Webster, C. L. Byard, *et. al*., Thin Solid Films **518**, 4935 (2010).
25. E. McKay, N.G. Pruiti, S. May, *et al.,* Sci Rep **13**, 19917 (2023).
26. H. El Dirani, L. Youssef, C. Petit-Etienne, *et. al.*, Opt. Express **27**, 30726 (2019).
27. J. Liu, G. Huang, R. N. Wang, *et al.,* Nat Commun **12**, 2236 (2021).
28. C. I. van Emmerik, W. A. P. M. Hendriks, M. M. Stok, *et al*., Opt Mater Express**10**, 1451 (2020).